Supporting Information

Selective CO production via dual-defective CdS/BiOCl photocatalyst for CO_2 photoreduction

Chuan Tan, Lili Ai *, Luxiang Wang *, Mengjiao Xu, Nannan Guo, Dianzeng Jia

State Key Laboratory of Chemistry and Utilization of Carbon Based Energy Resources, College of Chemistry, Xinjiang University, Urumqi, 830017, Xinjiang, PR China.

S1 Preparation of photocatalysts

BiOCl and CdS: 0.1 mmol of $Bi(NO_3)_3 \cdot 5H_2O$ and 0.1 mmol of KCl were dispersed in 60 mL deionized water before sonication for 10 min. Then, the solution was transferred to a 100 mL autoclave and kept at 120 °C for 10 h. After cooling, the sample was collected by centrifugation and washed 3 times with deionized water and ethanol, respectively. Finally, the sample was dried for 15 h by freeze-drying and the as-prepared sample was named as BiOCl. Similarly, 2.4 mmol $Cd(CH_3COO)_2 \cdot 2H_2O$ and 3.6 mmol CH_4N_2S were dispersed in 60 mL deionized water before sonication for 10 min. Then, the sample can be obtained by the similar preparation process of BiOCl sample, which was denoted as CdS.

BiOCl with oxygen vacancies: 0.1 mmol of $Bi(NO_3)_3 \cdot 5H_2O$, 0.1 mmol of KCl and 0.1 g of glucose were dispersed in 60 mL absolute ethanol before sonication for 10 min. Then, the solution was transferred to a 100 mL autoclave and kept at 160 °C for 24 h. Finally, the sample can be obtained by the similar preparation process of BiOCl sample, which was denoted as OV-B.

CdS with sulfur vacancies: 2.4 mmol $Cd(CH_3COO)_2 \cdot 2H_2O$ and 3.6 mmol CH_4N_2S were dispersed in

60 mL absolute ethanol before sonication for 10 min. Then, the solution was transferred to a 100 mL autoclave and kept at 200 °C for 24 h. Finally, the sample was denoted as SV-C.

None-defective BiOCl/CdS photocatalysts: 0.1 mmol of $Bi(NO_3)_3 \cdot 5H_2O$, 0.1 mmol of KCl, and 50 mg of as-prepared CdS sample were dispersed in 60 mL deionized water before sonication for 10 min. Then, the sample can be obtained by the similar preparation process of BiOCl sample, which was denoted as BiOCl/CdS.

Mono-defective BiOCl/CdS photocatalysts: 0.1 mmol of $Bi(NO_3)_3 \cdot 5H_2O$, 0.1 mmol of KCl, 0.1 g of glucose and 50 mg of as-prepared SV-C or CdS sample were dispersed in 60 mL absolute ethanol before sonication for 10 min. Then, the solution was transferred to a 100 mL autoclave and kept at 120 °C for 10 h and 160 °C for 24 h, respectively. Finally, the samples can be obtained by the similar preparation process of BiOCl sample, which was denoted as B/SV-C and OV-B/C.

Dual-defective BiOCl/CdS photocatalysts: 0.1 mmol of $Bi(NO_3)_3 \cdot 5H_2O$, 0.1 mmol of KCl, 0.1 g of glucose and different amount of as-prepared SV-C (10 mg, 50 mg, 70mg) were dispersed in 60 mL absolute ethanol before sonication for 10 min. Finally, the sample can be obtained by the similar preparation process of OV-B sample, which was denoted as OV-B/SV-C-1, OV-B/SV-C, OV-B/SV-C-3.

Causes of oxygen or sulfur vacancy formation: i) Reaction temperature: The strong Bi-O bonds in BiOCl and Cd-S bonds in CdS necessitate a sufficiently high reaction temperature for the construction of O or S vacancies. Temperatures of 160 or 200 ℃ may be critical, as they not only ensure adequate contact and interaction between reactants but also facilitate the migration and diffusion of O or S atoms, thereby leading to the formation of O or S vacancies within BiOCl or CdS crystals. ii) Solvent type: The

low boiling point of ethanol allows it to create a higher reaction pressure as a solvent, which is significant for the formation of O or S vacancies. Different solvents exhibit varying polarities and dissolution capacities, influencing the solubility and reaction rates of the reactants, and consequently affecting the structure and properties of the resultant products. In ethanol solvents, O or S atoms may migrate more readily from BiOCl or CdS crystals, promoting the formation of O or S vacancies. iii) Reaction time: The duration of the reaction also plays a crucial role in the formation of O or S vacancies. An insufficient reaction time may prevent complete interaction of the reactants, while an excessively prolonged reaction time could lead to a reduction or elimination of the vacancy count.

S2 Characterization

The crystal information of samples was obtained by X-ray diffraction (XRD, Cu Kα, Rigaku, Japan). The morphological and structural information were obtained using a field emission scanning electron microscopy (FESEM, Hitachi S-4800, Japan) and high-resolution transmission electron microscopy (HRTEM), respectively. The optical and adsorption property were measured by the UV-vis spectrophotometer (Hitachi U-3010, Japan). The photoluminescence (PL) spectra were obtained by a Hitachi fluorescence spectrophotometer (F-4500, Japan). The elemental composition was investigated by X-ray photoelectron spectroscopy (XPS, Thermo ESCALAB 250Xi, USA). The electron paramagnetic resonance (EPR) data was obtained by an EPR spectrometer (JES X320 JEOL Co.). The Fourier transform infrared (FT-IR) spectra were recorded on a spectrometer (FTIR-5700, Thermo, USA) with a wavenumber of 4000~400 cm^{-1}. Chemical impedance spectra (EIS), Mott−Schottky (MS), photocurrent were measured in a 0.5 M Na_2SO_4 solution via a standard three-electrode system where Pt plate, Ag/AgCl/saturated KCl (SCE) and an FTO plate coated with the sample were used as the counter

electrode, reference electrode and working electrode, respectively.

S3 Photoreduction performance

CO_2 photoreduction: Typically, 30 mg of the sample was added into 50 mL mixed solution of H_2O and MeCN (Volume ratio=4:1) and ultrasonicated for 1 min. Then, above solution was added into the reactor and CO_2 gas with high purity was used under xenon lamp (PLS-SXE 300D, 300 W, Perfectlight, China). The catalytic reduction products of CO_2 were monitored and collected on a gas chromatograph with an FID detector and a TCD detector (Agilent GC-7890B).

Cr(VI) photoreduction: In a typical process,10 mg ofphotocatalyst was added into a quartz tube reactor containing 30 mL of Cr (VI) solution (10 mg L^{-1}). In order to ensure the establishment of an adsorption-desorption equilibrium, the suspension was sonicated for 10 min and magnetically stirred in the dark for 30 min before irradiation. During the reaction process (LED light, RLH-54, 50W, Rogertech, 23 mW cm^{-2}), 1 mL aliquot of the suspension was taken out at given time intervals. The concentration of Cr (VI) ions in the supernatant was determined by the diphenylcarbazide (DPC) method and the corresponding UV-vis absorption spectra were recorded on a UV-vis spectrophotometer.

S4 Computational Details

Vienna ab initio Simulation Package (VASP) based on the Density Functional Theory (DFT) was used in all calculations.[1] The Plane-Wave basis sets with an adequate cutoff energy of 500 eV and accurate precision was used. Electron-ion core interactions were represented by the Projected Augmented Wave (PAW) approach,[2] while the General Gradient Approximation (GGA) of Perdew, Burke and Ernzerhof [4] (PBE) was used as the exchange-correlational functional to describe the

interactions among electrons. The Self-Consistence-Field (SCF) convergence criterion is 1 × 10−5 eV. The adsorption energies were calculated by using the following equation (1), [3]

$$E_{ads} = E_{total} - E_{sub} - E_{mol} \quad (1)$$

where Etotal is the total energy of substrates and adsorbates and E_{sub} is the energy of substrates and E_{mol} is the energy of adsorbed molecular. The gibbs free energy during reactions was defined as follows (2),[4]

$$\Delta G = \Delta E_{tot} + \Delta E_{ZPE} - T_{\Delta S} \quad (2)$$

Where ΔE_{tot} was the total energy, T was the room temperature chosen as 298.15 K, ΔE_{ZPE} was the zero-point energy change and ΔS was the difference in entropy.

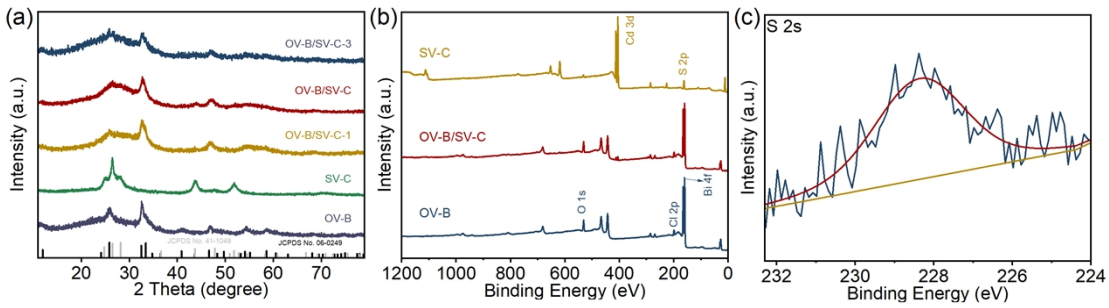

Figure S1. (a) XRD patterns of OV-B/SV-C-1 and OV-B/SV-C-3 samples, (b) XPS survey spectra of OV-B, SV-C and OV-B/SV-CV samples, (c) S 2s spectrum of OV-B/SV-C.

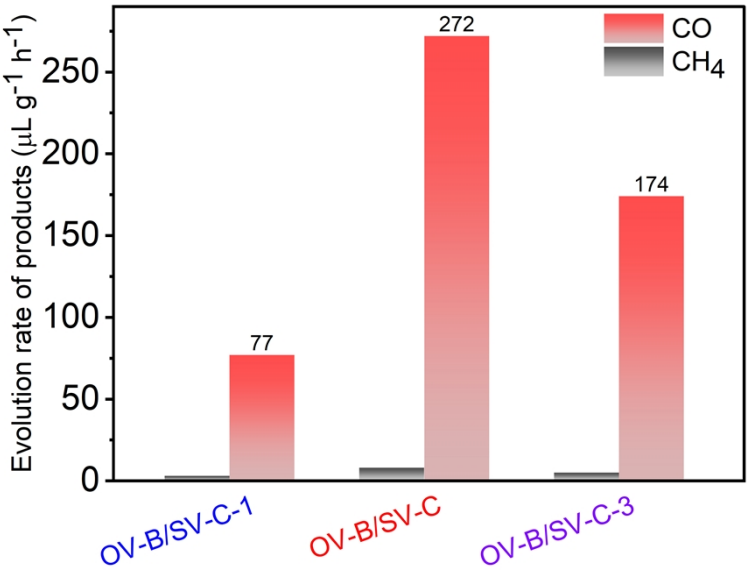

Figure S2. CO evolution rates of all samples prepared by adding different amount of SV-C

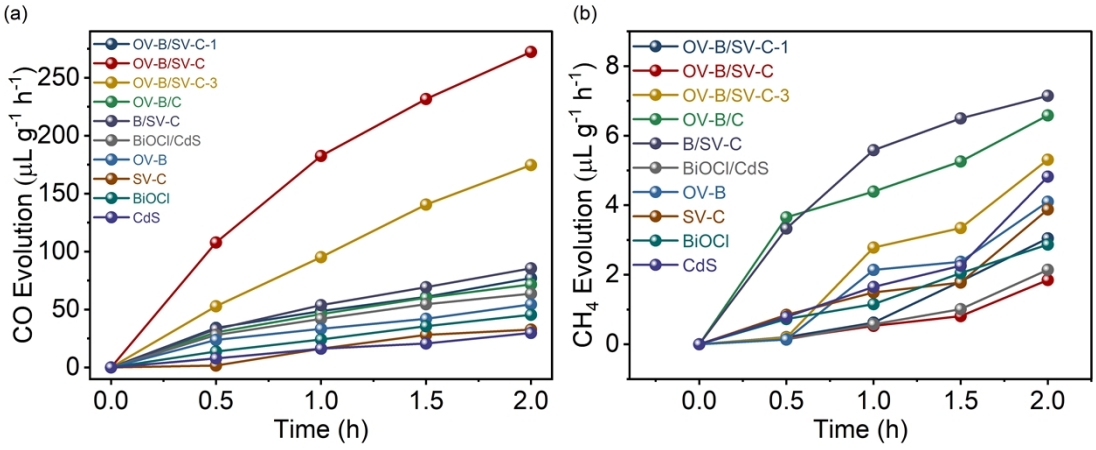

Figure S3. Evolution of products at different irradiation times: (a) CO and (b) CH_4 of as-prepared samples

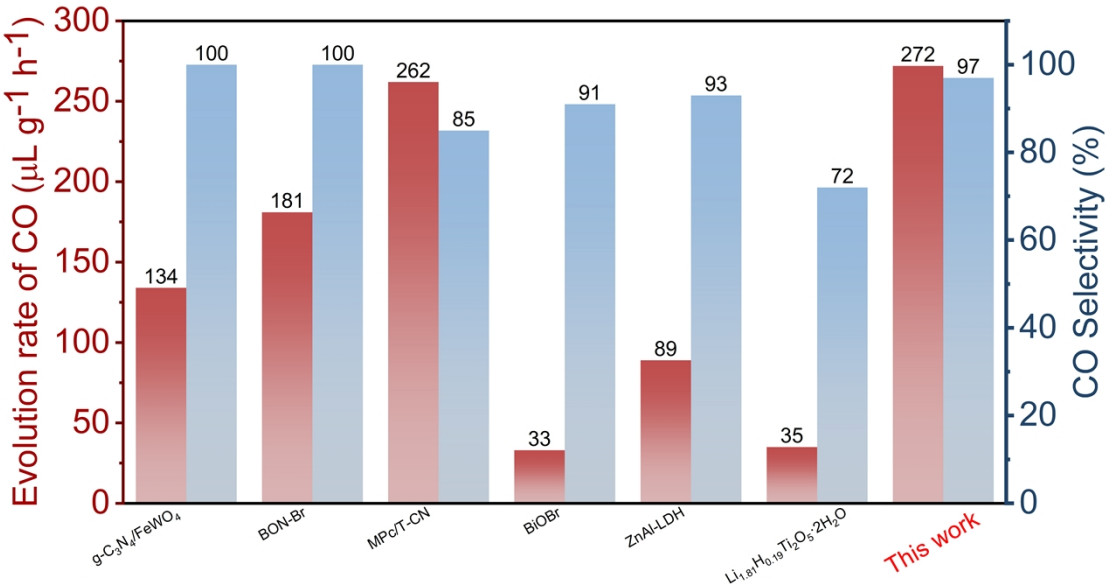

Figure S4. CO evolution rates and selectivity of recently reported phtocatalysts[5-10]

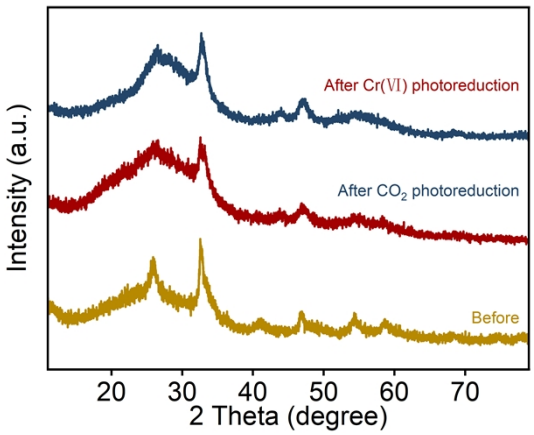

Figure S5. XRD patterns of OV-B/SV-C before and after photoreduction reaction

Table S1. Recently reported photocatalyst for removing Cr(VI) ions

Photocatalyst	Dosage (mg)	$C_{Cr(VI)}$ (mg/L)	Time	Light source	Degradation rate (%)	Ref.
Bi_2S_3/Ag	50	10	75 min	300 W Xe lamp	97	[11]
WO_3/In_2S_3	10	10	60 min	300 W Xe lamp	99	[12]
BiOBr-Bi_2S_3	75	10	12 min	500 W Xe lamp	100	[13]
FeC_2O_4/$Bi_{2.15}WO_6$	50	20	10 min	XPA-VII reactor	100	[14]
Bi_2S_3-ZnS/$MoSe_2$	20	40	3 h	500 W Xe lamp	95	[15]
UiO-66-NH_2	10	50	80 min	300 W Xe lamp	95	[16]
Cr-MOF/$ZnIn_3S_4$	40	50	30 min	300 W Xe lamp	95	[17]
Mo_2C/MoS_2/In_2S_3	50	40	90 min	350 W Xe lamp	99	[18]
Dual-Defective CdS/BiOCl	**10**	**10**	**1 min**	**50 W LED (425 nm)**	**100**	**This work**

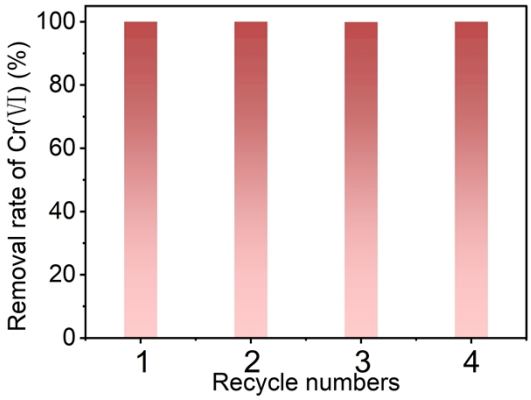

Figure S6. Recycling performance of Cr(VI) over OV-B/SV-C

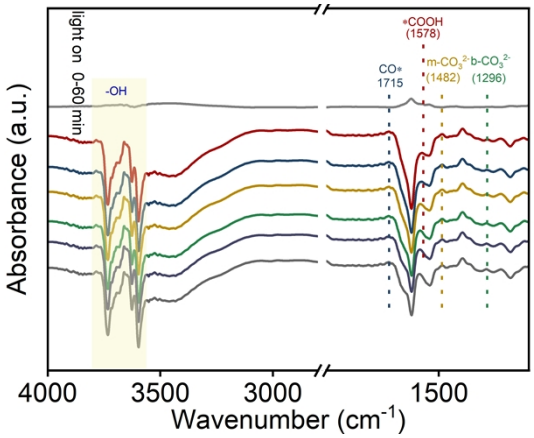

Figure S7. In situ FT-IR spectra of the OV-B/SV-C sample.

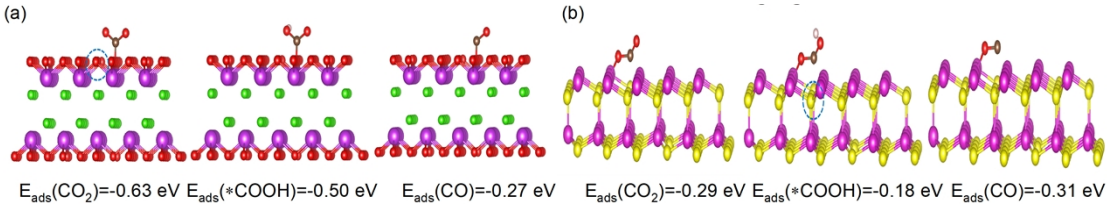

Figure S8. E_{ads} of the intermediate products on the photocatalyst surface over as-preprared samples: (a) OV-B; (b) SV-C

Table S2 Results of DFT calculation: ΔH, ΔG and G values of ∗CO_2, ∗COOH and ∗CO on as-prepared photocatalysts

	ΔH			ΔG			G		
	∗CO2	**∗COOH**	**∗CO**	**∗CO_2**	**∗COOH**	**∗CO**	**∗CO_2**	**∗COOH**	**∗CO**
OV-B	-0.43	0.56	1.23	-0.36	0.40	0.04	-0.79	0.96	1.27
SV-C	-0.10	0.55	1.06	-0.32	0.37	0.04	-0.42	0.92	1.10
OV-B/C	-0.82	0.33	0.63	-0.33	0.34	0.08	-1.15	0.67	0.71
B/SV-C	-0.70	0.41	0.59	-0.37	0.37	0.05	-1.07	0.78	0.64
OV-B/SV-C	-1.48	0.15	0.40	-0.38	0.36	0.05	-1.86	0.51	0.45

Notes and references

1. Grimme, S.; Antony, J.; Ehrlich, S.; Krieg, H., A Consistent and Accurate Ab Initio Parametrization of Density Functional Dispersion Correction (DFT-D) for the 94 Elements H-Pu. *J. Chem. Phys.* **2010,** *132*, 154104.

2. J. K. Nørskov; J. Rossmeisl; A. Logadottir; Lindqvist, L., Origin of the Overpotential for Oxygen Reduction at a Fuel-Cell Cathode. *J. Chem. Phys.* **2004,** *108*, 17886-17892.

3. Kresse, G.; Joubert, D., From ultrasoft pseudopotentials to the projector augmented-wave method. *J. Chem. Phys.* **1999,** *59*, 1758.

4. P., J.; Perdew; Kieron Burke; Ernzerhof, M., Generalized Gradient Approximation Made Simple. *Phys. Rev. Lett.* **1996,** *77*, 3865-3868.

5. Bhosale, R.; Jain, S.; Vinod, C. P.; Kumar, S.; Ogale, S., Direct Z-Scheme g-C_3N_4/$FeWO_4$ Nanocomposite for Enhanced and Selective Photocatalytic CO_2 Reduction under Visible Light. *ACS Applied Materials & Interfaces* **2019,** *11*, 6174-6183.

6. Sun, J.; Bian, J.; Li, J.; Zhang, Z.; Li, Z.; Qu, Y.; Bai, L.; Yang, Z.-D.; Jing, L., Efficiently Photocatalytic Conversion of CO_2 on Ultrathin Metal Phthalocyanine/g-C_3N_4 Heterojunctions by Promoting Charge Transfer and CO_2 Activation. *Applied Catalysis B: Environmental* **2020,** *277*.

7. Wu, D.; Ye, L.; Yip, H. Y.; Wong, P. K., Organic-Free Synthesis of {001} Facet Dominated BiOBr Nanosheets for Selective Photoreduction of CO_2 to CO. *Catalysis Science & Technology* **2017,** *7*, 265-271.

8. Xue, J.; Yu, Y.; Yang, C.; Zhang, K.; Zhan, X.; Song, J.; Gui, J.; Li, Y.; Jin, X.; Gao, S.; Xie, Y., Developing Atomically Thin $Li_{1.81}H_{0.19}Ti_2O_5 \cdot 2H_2O$ Nanosheets for Selective Photocatalytic CO_2 Reduction to CO. *Langmuir* **2021,** *38*, 523-530.

9. Zhao, J.; Lu, Y.; Wu, D.; Qin, Y.; Xie, Y.; Guo, Y.; Raza, W.; Luo, G.; Asim Mushtaq, M.; Wu, Y.; Mu, X.; Ling, Y.; Ilyas, T.; Ul Hassan, Q.; Gao, C., Regulating Divalent Metal Species in Aluminum-Based Layered Double Hydroxides to Selectively Promote Photocatalytic CO Production from CO_2. *Sep. Purif. Technol.* **2023,** *305*, 122508.

10. Hao, L.; Kang, L.; Huang, H.; Ye, L.; Han, K.; Yang, S.; Yu, H.; Batmunkh, M.; Zhang, Y.; Ma, T., Surface‐Halogenation‐Induced Atomic‐Site Activation and Local Charge Separation for Superb CO_2 Photoreduction. *Advanced Materials* **2019,** *31*, 1900546.

11. Cao, J.; He, J.; Ye, J.; Ge, K.; Zhang, Y.; Yang, Y., Urchin-Like Bi_2S_3/Ag Nanostructures for Photocatalytic Reduction of Cr(VI). *ACS Applied Nano Materials* **2021,** *4* (2), 1260-1269.

12. Hua, Y.; Hu, C.; Arif, M.; Chen, S.-m.; Zhang, M.; Liu, X., Direct Z-Scheme WO_3/In_2S_3 Heterostructures for Enhanced Photocatalytic Reduction Cr(VI). *Journal of Alloys and Compounds* **2022,** *908*.

13. Long, Z.; Zhang, G.; Du, H.; Zhu, J.; Li, J., Preparation and Application of BiOBr-Bi_2S_3 Heterojunctions for Efficient Photocatalytic Removal of Cr(VI). *Journal of Hazardous Materials* **2021,** *407*.

14. Pan, Z.; Cai, C.-C.; Li, T.-T.; Lou, C.-W.; Lin, J.-H.; Ren, H.-T., Multipath Collaboration Mechanisms Involved in the Photocatalytic Reduction of Cr(VI) by $FeC_2O_4/Bi_{2.15}WO_6$. *Journal of Photochemistry and Photobiology A: Chemistry* **2023,** *445*.

15. Qiu, L.; Wang, Y.; Zhu, C.; Tian, F.; Zhang, X.; Huang, D.; Sheng, J.; Yu, Y.; Yang, W., Designing a Novel Dual Z-Scheme Bi_2S_3-ZnS/$MoSe_2$ Photocatalyst for Photocatalytic Reduction of Cr(VI). *Separation and Purification Technology* **2022,** *286*.

16. Ren, J.; Tao, L.; Luo, Z.; Yin, D., Defective UiO-66-NH_2 Design with Enhanced Photocatalytic Reduction of Cr(VI). *New Journal of Chemistry* **2024,** *48* (9), 3818-3828.

17. Zhang, L.; Qiu, J.; Dai, D.; Zhou, Y.; Liu, X.; Yao, J., Cr-Metal-Organic Framework Coordination with $ZnIn_2S_4$ Nanosheets for Photocatalytic Reduction of Cr(VI). *Journal of Cleaner Production* **2022,** *341*.

18. Zhang, X.; Tian, F.; Qiu, L.; Gao, M.; Yang, W.; Liu, Y.; Yu, Y., Z-Scheme $Mo_2C/MoS_2/In_2S_3$ Dual-Heterojunctions for the Photocatalytic Reduction of Cr(VI). *Journal of Materials Chemistry A* **2021,** *9* (16), 10297-10303.